An Edge-Slotted Waveguide Array with Dual-Plane Monopulse

Richard R. Kinsey, *Life Senior Member, IEEE*

***Abstract*— Edge-slotted row waveguides have often been stacked to form light-weight planar arrays. With phase-shifter scanning in elevation and 360° mechanical rotation in azimuth, a large surveillance volume may be covered at relatively low cost. For applications that require accurate target location, elevation monopulse is readily available by means of an appropriate beamformer. However, past attempts to obtain monopulse in the plane of the slotted waveguides have not met with much success. While the alternative has been to employ run length estimation (beam-splitting based on a sequence of target returns), accuracy limitations and the required elevation dwell time render this solution inadequate for certain applications. Now, however, a new waveguide array configuration has been developed that provides dual-plane monopulse and still retains one-dimensional phase scanning along with the advantages of low cost and light weight. A full-scale *Ku*-band array employing this new architecture has been built and tested to demonstrate practical utility.**

***Index Terms*— Array antenna, dual-plane monopulse, edge-slotted waveguide.**

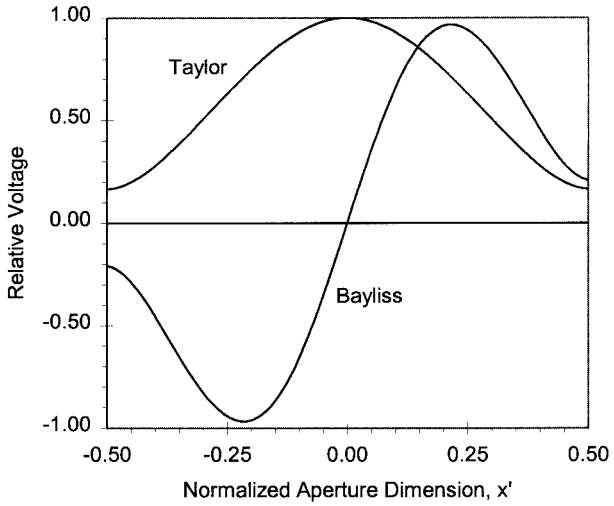

Fig. 1. Independent sum and difference amplitude tapers.

I. Introduction

PRIOR attempts to obtain monopulse from traveling-wave arrays have usually involved forming a pair of overlapped pencil beams that are combined in a hybrid to obtain sum and difference outputs. This pair of pencil beams may be obtained from a pair of interleaved slotted waveguide arrays having different beam squints [1] or by slotted waveguides that operate in either of two different modes of excitation with separate hybrid ports for each mode [2]. A significant limitation of these overlapped beam techniques is their rather poor monopulse gain and angular sensitivity performance. This is a result of the equivalent sum and difference array excitations being so far removed from ideal independent amplitude tapers. With pencil beams overlapped at their −3-dB points, additional losses are computed to be on the order of 1.6 dB in gain and 3 dB in angular sensitivity as compared to independent Taylor [3] and Bayliss [4] amplitude tapers.

A second monopulse approach involving interleaved arrays can be implemented with an even (sum) excitation on one array and an odd (difference) excitation on the other [5], as in Fig. 1. The aperture field components contributing to the monopulse sum and difference signals are then separated in the array aperture itself. Since these two excitations are orthogonal to one another, the sum beam gain and the difference pattern error slope can each be realized without any additional loss due to the presence of the other interleaved array. In contrast to the technique of forming monopulse from a pair of overlapped beams, the beam squint for sum and difference interleaved arrays is designed to be the same for both. This has the advantage that the waveguide propagation velocity and slot spacing for both arrays may also be the same with the result that sum and difference patterns remain coincident with changes in RF frequency. However, it has the disadvantage that only one of the interleaved arrays (and consequently only one half the array phase shifters) is used on transmit. This may impose an undesired limitation on transmitter power, especially at the higher microwave frequencies, or else unnecessarily increase phase-shifter costs.

II. A New Approach to Monopulse Capability

The monopulse stick phased array (MSPA) aperture is formed by interleaving two arrays of sticks (end-fed, edge-slotted traveling-wave-type elements). However, in this case, the excitations for the two arrays are each derived from a combination of independent sum and difference amplitude tapers [6]. In order to double the RF power capability of the antenna, by utilizing all the array phase shifters on transmit all sticks must couple to both even and odd field components.

If $f_o(x')$ is the excitation for the interleaved array of odd numbered sticks and $f_e(x')$ is the excitation for the interleaved array of even numbered sticks, then two candidate excitations

Manuscript received May 28, 1997; revised May 20, 1998. The development and fabrication of the antenna was performed under Navy Contract N60921-93-C-A202.

The author is with Sensis Corporation, DeWitt, NY 13214 USA.

Publisher Item Identifier S 0018-926X(99)04443-9.

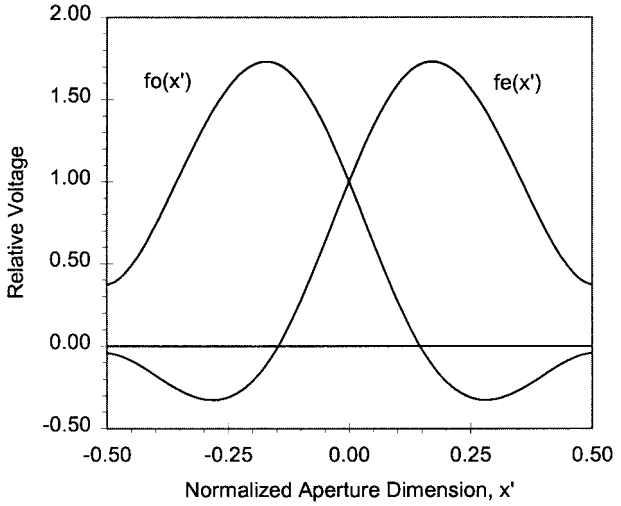

Fig. 2. Odd and even stick excitations.

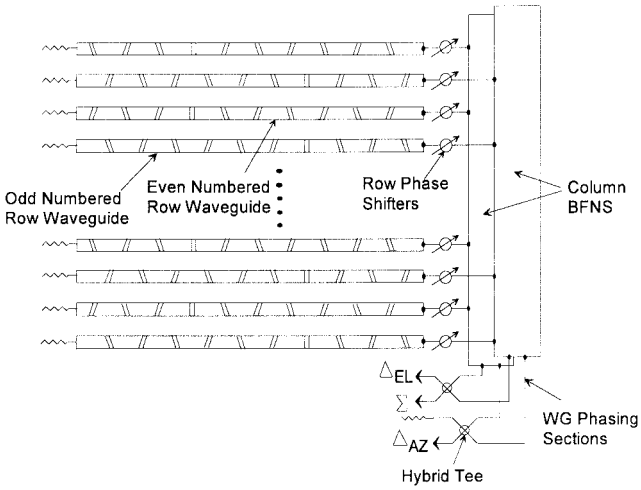

Fig. 3. Block diagram of array architecture.

that fulfill this objective can be expressed in canonical form as

$$f_o(x') = f_\Sigma(x') - f_\Delta(x') \quad (1)$$

$$f_e(x') = f_\Sigma(x') + f_\Delta(x') \quad (2)$$

where $-0.5 \leq x' \leq 0.5$.

Fig. 2 illustrates the $f_o(x')$ and $f_e(x')$ derived from 35-dB Taylor and Bayliss amplitude tapers. Since the $f_o(x')$ and $f_e(x')$ are the arithmetic sum and difference of the Taylor and Bayliss amplitude tapers, they yield real rather than complex excitations.

Note that the excitation amplitude of a waveguide edge slot is controlled by the angle of the slot tilt and that changing the tilt from a+angle to a−angle introduces a 180° phase change in this excitation. Since the $f_o(x')$ and $f_e(x')$ excitations both enjoy the same linear beam squint, the slot spacing is uniform and the additional 180° phase change required at the point where an excitation goes negative is simply introduced by a change in the order of the slot tilts. Combining each pair of neighboring sticks (odd and even) in a 3-dB hybrid recovers the row-pair Σ and Δ outputs. However, for a scanning array, these row-pair Σ and Δ outputs can instead be formed on the *transmitter* side of the phase shifters. In this case, *all* phase shifters share the transmit power thereby doubling the array RF power capability. Monopulse in the plane orthogonal to the sticks is obtained in the conventional manner by combining the individual linear array outputs in beamforming networks that form independent sum and difference patterns. By first combining all the odd rows and all the even rows in separate column beamforming networks (BFN's) as in Fig. 3, only a single pair of hybrid tees is required to combine the BFN ports and obtain the full monopulse set of $\Sigma, \Delta_{\text{az}}$ and Δ_{el}.

To avoid the appearance of visible space-grating lobes for a given beam scan requirement, it should be noted that the sticks in each of the two interleaved arrays must be spaced as they would be in a conventional array. Adjacent sticks in the aperture are, therefore, positioned at one half the usual spacing and this requires the use of reduced height waveguide to permit wide-angle scanning. It turns out that the range of slot conductance values versus tilt angle is not much different from full height waveguide even though more of the slot must occupy a cut back in the broadwall to achieve resonance.

Only a brief overview of the MSPA demonstration antenna will be provided here so that the results of recently completed testing may be presented. For a more complete description of the interleaved array concept and details of the antenna construction, the reader is referred to an earlier paper [7].

III. Demonstration Antenna

Rather than building a rotator as indicated by the schematic block diagram in Fig. 3, the demonstration MSPA antenna was specified by our customer to be at *Ku*-band and sized to mount within a Phalanx Radar Servo Structure (RSS) in place of the existing track reflector. A photograph of the completed antenna is shown in Fig. 4.

Design goals were based on improved sidelobe performance with beamwidths and gain similar to the reflector antenna, while providing 70° to 90° of electronic scan in azimuth. The largest MSPA that could fit in place of the reflector and still assure minimum antenna clearances of 0.5 in under all possible gimbal motions was determined to be one having the stick inputs at the top of the aperture. A forward tilt of the aperture to compensate for mid-band beam squint, permits the available gimbal motion to accommodate the changes in beam squint over a 10% frequency band. The design goal for the total antenna weight was 50 lbs. This was successfully achieved and is broken down by major categories in Table I.

Several innovations that make the phasing/beamforming assembly very compact are illustrated in Fig. 5. First, the waveguide sticks incorporate an H-plane bend in the feed end so that the input ports are at the rear of the array rather than the top end of the sticks. This allows the odd and even arrays to have their flanges offset above and below each other and permits the same half-height waveguide flanges to be used throughout the array. The waveguide length differences resulting from the stagger in flange locations and the offset in the BFN's is equalized by the waveguide loops connecting the BFN feed ports to a pair of 3-dB hybrids at the rear.

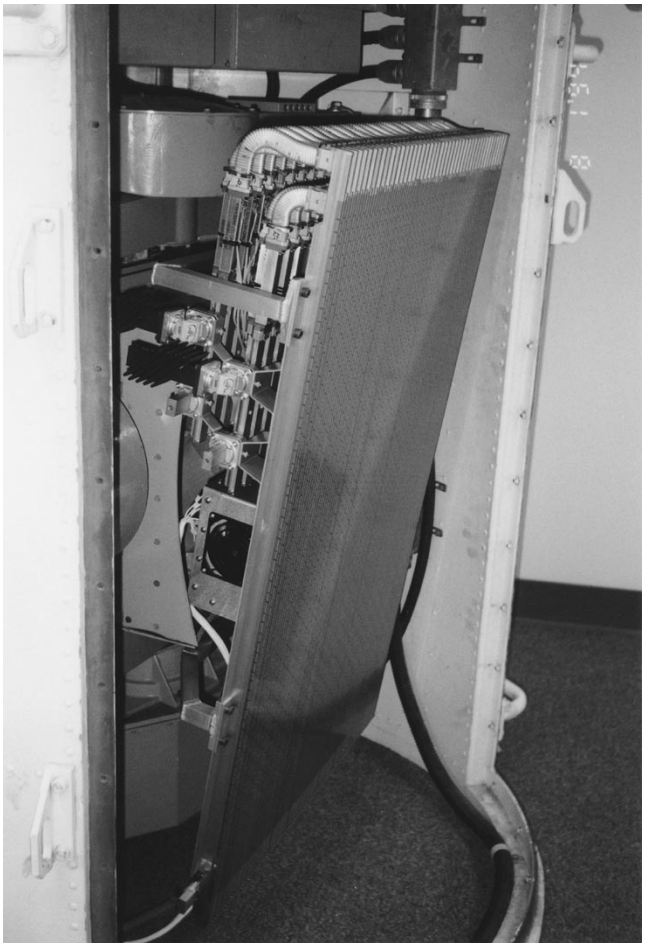

Fig. 4. The antenna installed in a Phalanx RSS with the radome removed.

TABLE I
ANTENNA COMPONENT WEIGHTS

Sticks	13.80
Aperture Backing Plate and Assembly Hardware	4.40
Flex Bends	5.44
Phase Shifters	8.58
Phase Shifter Driver Box	6.42
Azimuth BFN (incl. Hybrids)	6.41
Supports and Hardware	4.20
Total Measured Antenna Weight	49.25 lbs.

Second, the flange offset permits two identical BFN's to be used with their corresponding Σ and Δ ports offset the exact amount necessary to mate with a standard hybrid-tee panty adapter. This simplifies the waveguide runs and minimizes the depth of the beamforming assembly. The transmit power is divided equally between the two BFN's which each provide a large area heat sink for the phase shifter and feed losses. At the load ends of the BFN's, ambient air-cooled waveguide loads must each handle only $1/2$ the total mainline waster load loss.

Third, the waveguide twist normally required between the stick ports and the BFN ports is incorporated in the phase shifter itself at no additional length. This is possible with dual-mode reciprocal phase shifters, which have circular polarizers at either end and the orientation of the waveguide interface is

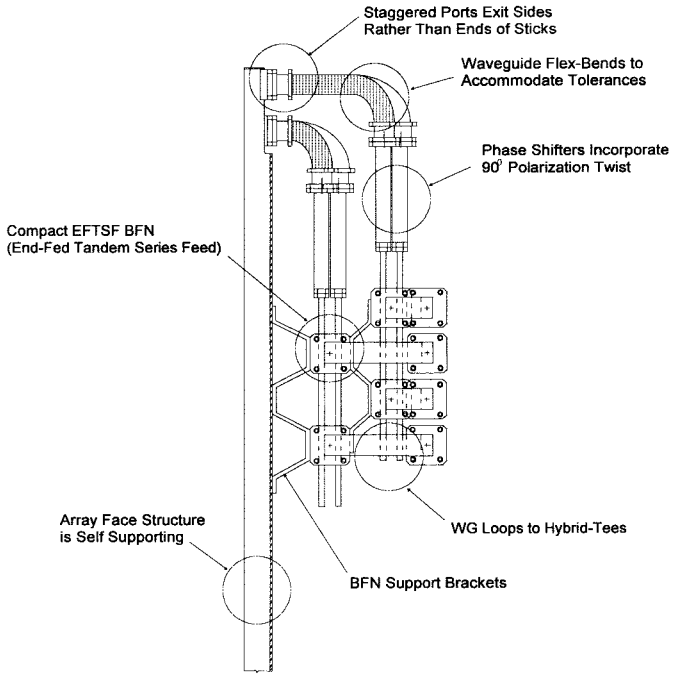

Fig. 5. Side view of array component packaging.

arbitrary. While the length of the array phase shifters was only 3.5 in, note that they could have been either shorter or longer without affecting the basic design layout.

Finally, waveguide phasing loops between the BFN's and the hybrids at the rear can easily be shimmed if necessary to correct errors in electrical path length.

IV. ANTENNA TEST RESULTS

Measurements at the Naval Research Laboratory (NRL) Compact Range Facility were taken with the array mounted on an $az/el/az$ positioner and pattern cuts were recorded with clockwise azimuth rotation (as viewed from above). In general, patterns were recorded over a $\pm 60°$ range about broadside in nominal steps of 0.25°. However, difference pattern null regions were recorded in smaller steps of 0.05° in order to more accurately determine the boresight null depths.

The phase tables used by the beam steering controller (BSC) to collimate the array were generated by a Fortran code that predicted the insertion phase of the waveguide sticks, flexible bends, the BFN's, and waveguide runs to the hybrids at arbitrarily chosen frequencies. The code is based on theoretical propagation phase but utilizes mid-band and in some cases end-of-band component measurements taken prior to array construction. The phase shifters had their own separate phase tables, which were derived from phase data measured by the manufacturer at five frequencies and at temperatures of 0°, 30°, and 60°C.

Primarily because of time constraints, all array patterns were measured using the original phase tables. No pattern range phase measurements were made to improve the array collimation corrections (range tuning). In the phase scan plane (azimuth), the phase shifters appear to be the dominant error source and lower azimuth sidelobes could undoubtedly

Fig. 6. MSPA antenna aligned for an E-plane pattern in the azimuth plane.

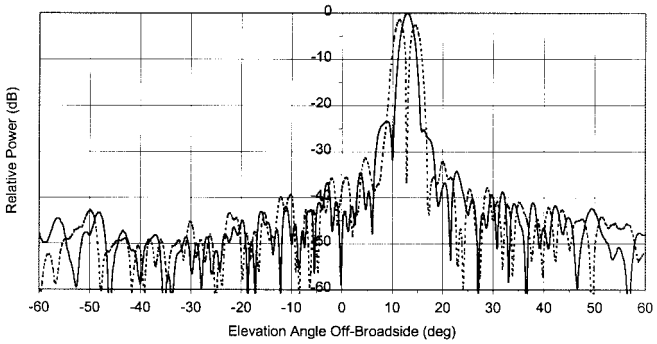

Fig. 7. E-plane monopulse patterns at FL.

be realized if range tuning was employed. On the other hand, elevation plane patterns are virtually independent of row combining errors and, thus, fairly represent the array performance at its present state of development.

A. Elevation Patterns

Principal elevation (E-plane) patterns were recorded by turning the array 90° about the mounting axis (Fig. 6) and rotating it in azimuth. It was necessary to do this to obtain patterns over a wide E-plane angle since rotation of the positioner in the vertical plane was limited for angles below the horizontal. Patterns were recorded for five equally spaced frequencies covering a 10% band. Those at the low, mid, and high end of the band have been designated by FL, FM, and FH, respectively, and are shown in Figs. 7–9. The sum and difference patterns were separately recorded but have been overlaid on the same plot for each frequency with the sum peak normalized to 0 dB. Sum and difference sidelobes are below −30 dB except for the first sum sidelobe at about −23 dB. Patterns computed during the design phase that modeled the change in slot conductance with frequency exhibited similar first sidelobe ratios (Table II).

Difference patterns throughout the frequency band exhibit boresight null depths of about −37 dB. One conclusion that can be drawn from this excellent performance is that the boresight gains of the two interleaved arrays (including losses

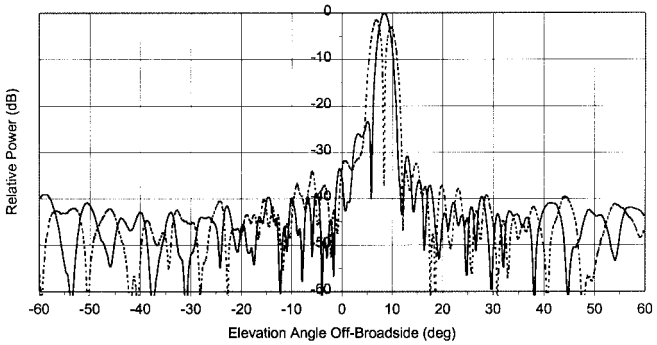

Fig. 8. E-plane monopulse patterns at FM.

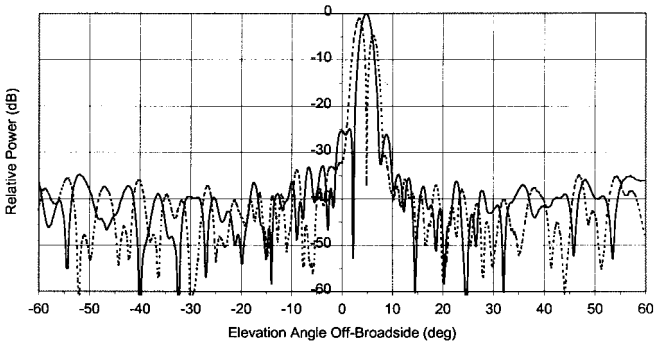

Fig. 9. E-plane monopulse patterns at FH.

TABLE II
COMPUTED NO-ERROR DESIGN PATTERN SIDELOBES

Freq	1st Σ SLR dB	1st Δ SLR dB
FL	22.4	33.6
FM	34.7	40.8
FH	21.7	31.2

in the phase shifters, BFN and waveguide runs) must be equal to within 0.25 dB.

The beam squint (in the plane of the sticks), as obtained from the measured elevation patterns, is plotted in Fig. 10 together with the beam squint computed from the following:

$$\sin\theta_s = \left(\frac{\lambda}{\lambda_g} - \frac{\lambda}{2s}\right) \tag{3}$$

where $s =$ slot spacing, λ is free-space wavelength, and λ_g is guide wavelength. Note that the sticks are fed from the top so that $-\theta_s$ is a positive elevation angle.

The stick a dimension is 0.622 in with a measured root mean square (rms) accuracy of 0.001 in. However, the capacitive susceptance due to the slot wall thickness and mutual coupling effects reduces the phase velocity so that the effective a dimension is somewhat larger. The guide wavelength computed for an effective waveguide width of 0.6337 in gives a result that closely matches the measured beam squints (Fig. 10).

B. Azimuth Patterns

Azimuth patterns were recorded over the 10% band with the array oriented normally. The antenna mounting structure

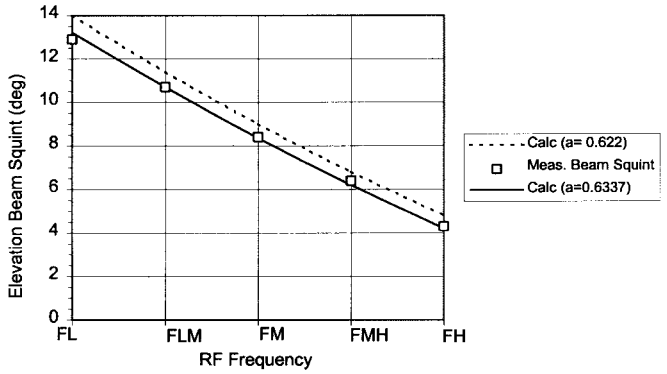

Fig. 10. Elevation beam squint.

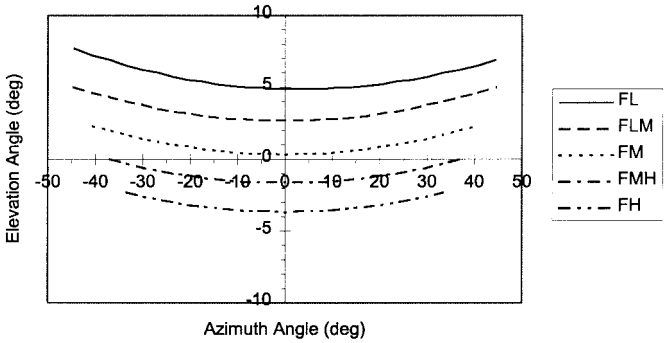

Fig. 11. Azimuth and elevation angles with beam scan.

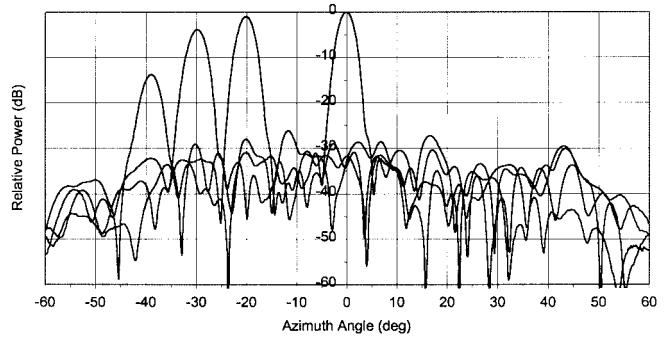

Fig. 12. Azimuth plane cuts at FM for several beam scans.

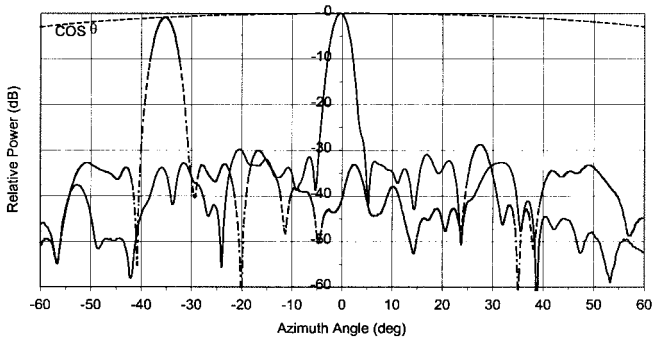

Fig. 13. Azimuth pattern cut through the scan cone at 35°.

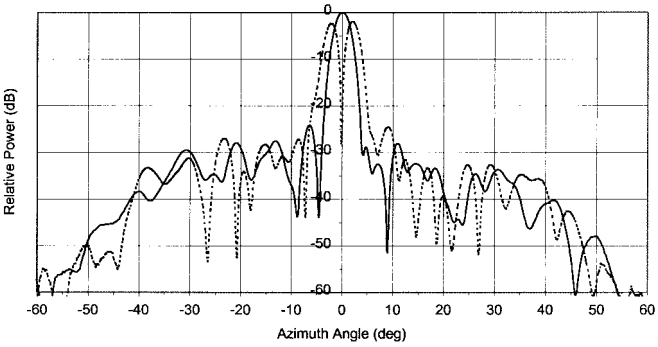

Fig. 14. Azimuth monopulse patterns at FL.

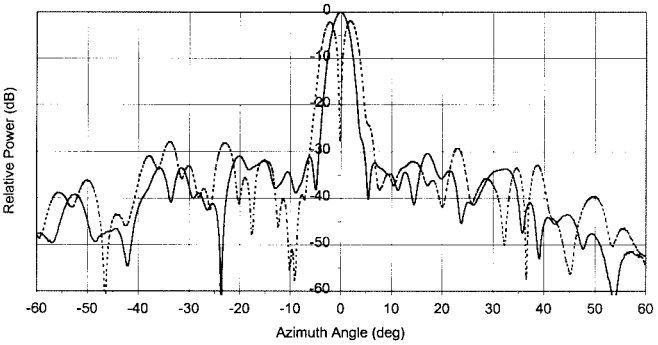

Fig. 15. Azimuth monopulse patterns at FM.

provides an 8° forward tilt of the aperture to compensate for the mid-band elevation beam squint. Because of this beam squint, a phase-scanned beam follows a conical path in angle space as shown by the plots in Fig. 11 for five equally spaced frequencies over the 10% band. In addition to the azimuth and elevation angles, the width of each plot indicates the maximum allowable array scan (for a grating lobe at endfire).

With the array tilted forward, to position the main beam at 0° elevation, azimuth patterns were recorded for several different H-plane phase scans. An overlay of these patterns is shown in Fig. 12. However, as indicated in Fig. 11, the scanned beam pulls away in elevation from the azimuth plane so that azimuth patterns begin to cut through the side of the scanned beam rather than the nose. The main beam scan loss is much less than the exaggerated reduction indicated by these off-axis pattern cuts.

To observe the actual scan loss, the forward tilt of the array aperture must be adjusted so that an azimuth pattern passes through the nose of the scanned beam. This was done for a scan of 35° at frequency FM and the resulting pattern is overlaid on a broadside pattern in Fig. 13, together with a $\cos\theta$ falloff. The actual principal cone-scan loss is very close to the loss in projected aperture (within 0.1 dB for this test).

Azimuth patterns are shown in Figs. 14–16 for frequencies FL, FM, and FH. The sum and difference patterns were separately recorded but have been overlaid at each frequency with the sum peak normalized to 0 dB. Peak sidelobes are -25 to -30 dB, even without the benefit of range tuning.

C. Off-Axis Patterns

The array aperture excitations are the product of row and column amplitude tapers. Off axis in elevation, azimuth sidelobes are suppressed by the stick patterns and quickly drop to

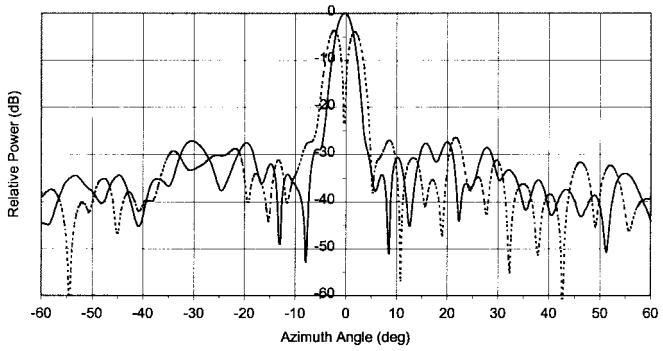

Fig. 16. Azimuth monopulse patterns at FH.

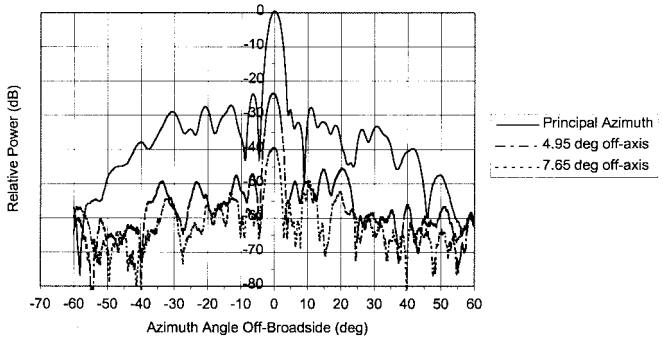

Fig. 17. Azimuth cuts off-axis in elevation.

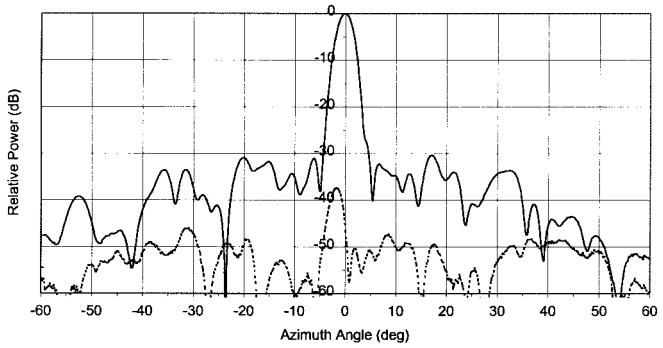

Fig. 18. Co-pol and X-pol azimuth plane patterns at FM.

the -60-dB level (≈ -25 dBi) as shown by the pattern cuts in Fig. 17 recorded at FL.

D. Cross-Polarization Response

A potentially undesirable characteristic of waveguide arrays is the cross-polarization response from the tilted edge slots. In the MSPA demonstration antenna this response was minimized in two ways. First, by optimizing the location of a short circuit in the trough between the sticks and second, by making the starting tilt angles of slots in alternate odd or alternate even sticks opposite to one another. Changing the starting tilt angle requires that 180° of compensating phase shift be added to maintain principal polarization phase coherence; it also makes the cross-polarized components from neighboring slots of either array 180° out of phase with one another so that they tend to cancel in the principal planes. A measured

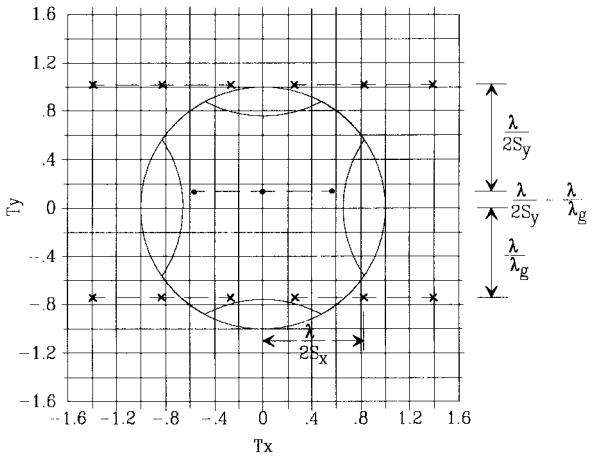

Fig. 19. T-plane scan locations of main beam and X-pol lobes.

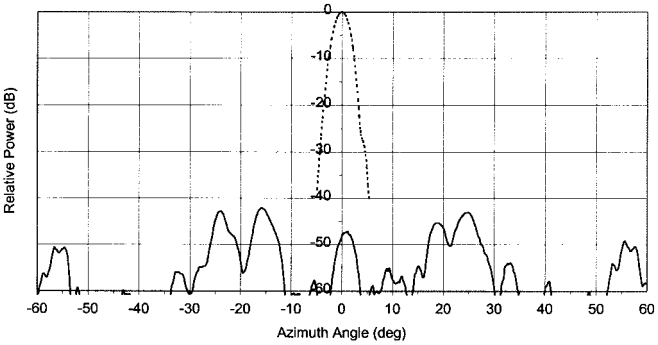

Fig. 20. Azimuth sum beam cut through theoretical X-pol peak at 25°.

X-pol pattern, in the plane orthogonal to the sticks, is shown in Fig. 18 and is down 37 dB or more from the peak of the principally polarized main beam.

At particular angles off axis, as shown by the T-plane plot (sine-theta space) in Fig. 19, the X-pol fields from the alternating slot tilts become cophased and tend to produce an undesired X-pol lobe. This plot shows the main beam (solid circle) at FM as it is scanned $\pm 35°$. The theoretical location of the X-pol lobe peaks for either interleaved array are indicated by X's on the plot and these scan in unison with the main beam as indicated. At the azimuth broadside position, all four of these X-pol lobes are suppressed by virtue of the fact they are all outside the unit circle (visible space). With azimuth scan, only one of the two lower X-pol lobes can enter visible space at a time and neither of the two top X-pol lobes ever appears.

From the coordinate relations between angle space and T-plane space, the location of the X-pol lobe for either of the two interleaved arrays can be computed. For a principal cone main-beam scan of 35°, at the mid-band frequency FM this X-pol lobe should occur at $-26°$ azimuth, $-54.5°$ elevation. The maximum sum port X-pol response that was found in this region occurred at $-52.5°$ elevation and was over 40 dB down. An azimuth X-pol pattern cut at this elevation is shown in Fig. 20 with the principal pol main beam added as a reference (note that pattern angles are the negative of actual azimuthangles).

TABLE III
DIRECTIVITY AND GAIN PREDICTIONS

	FL	FM	FH
Area Gain	40.19	40.65	41.08
Azimuth Taper Gain Factor	-1.01	-1.16	-1.38
Stick (pair) Taper Gain Factor	-1.10	-1.14	-1.35
Error Effects	-0.10	-0.10	-0.10
Directivity (dB)	37.98	38.37	38.25
Ohmic Losses			
Stick WG	0.19	0.18	0.17
Stick load	0.62	0.17	0.34
Flex Bends	0.10	0.10	0.10
Phase Shifter	0.60	0.60	0.60
EFTSF (incl. loads)	0.90	0.70	0.70
Hybrid and WG Loops	0.16	0.15	0.14
Total	2.57	1.90	2.05
Array Gain (dB)	35.41	36.47	36.20

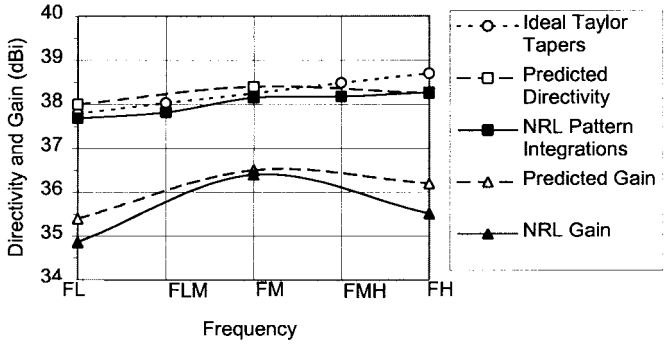

Fig. 21. Directivity and gain versus frequency.

TABLE IV
MONOPULSE ERROR SLOPES

Frequency	El. Bayliss/Taylor	Meas. Elevation	Az. Bayliss/Taylor	Meas. Azimuth
FL	0.0510 v/v/ms	0.0484 v/v/ms	0.0352 v/v/ms	0.0335 v/v/ms
FM	0.0537 v/v/ms	0.0492 v/v/ms	0.0371 v/v/ms	0.0338 v/v/ms
FH	0.0564 v/v/ms	0.0513 v/v/ms	0.0384 v/v/ms	0.0342 v/v/ms

TABLE V
ARRAY PERFORMANCE CHARACTERISTICS

Agile Bandwidth	10%
Monopulse	Az and El
Overall Aperture Size	.93 m vert x .60 m horiz
Active Aperture Size	.80 m vert x .55 m horiz
Polarization	Linear Vertical
Gain (Hybrid Σ Port)	36.4 dBi (at FM)
RF Frequency	Ku-Band
HPBWs	2.8° az x 2.0° el
Azimuth SLR	>25 dB
Elevation SLR (after 1st)	>30 dB
El Beam Squint (midband)	8.4°
Beam Squint Sensitivity	2/3°/100 MHz
No. Phase Shifters	84
Azimuth Phase Scan (midband)	±42° maximum
Beam-to-beam Sw Rate	1 kHz
Beam Re-phasing Time	80 μs
Max RF Power:	26 kWp, 800 Wa
Antenna Weight (meas)	49.25 lbs.

E. Array Directivity and Gain

Table III is a calculation of expected directivity and gain. The azimuth gain factor (amplitude taper efficiency) was computed from bench measurements of the BFN antenna port amplitudes and the elevation gain factor from near-field probing a pair of odd and even sticks. Ohmic losses were obtained from network analyzer measurements of the various array components.

The array directivities computed in Table III are plotted in Fig. 21 together with the ideal row–column Taylor taper directivities and the directivities obtained by integration of the NRL patterns. A two-dimensional pattern in T space was derived from the product of measured azimuth and elevation patterns. The off-axis sidelobe levels so obtained should be representative of actual values down to the noise floor set by the slot scattering level. This noise floor is so low that the differences between computed and actual values have a negligible impact on the total radiated energy. Directivities were obtained with T-plane integrations of about 20 000 points and on average these agree with the predicted directivities within 0.2 dB.

An NRL standard gain horn (SGH) was used to obtain system reference levels over the frequency band. Relating patterns to this reference level determined the dBi value at the pattern peaks and this is plotted as NRL gain for FL, FM and FH in Fig. 21. At a particular frequency, the same gain value should be obtained for either an E plane or an H plane cut through the beam peak. However, due to inexact mount realignment for changes in beam squint with frequency, pattern cuts were not always made exactly through the beam peaks. For differences of a few tenths of a decibels, the higher value was taken as being closer to the true beam peak.

F. Monopulse-Error Slopes

The boresight error slope of Δ/Σ in v/v/ms (where ms = millisines) was obtained from the measured sum and difference patterns. These slopes are summarized in Table IV along with the ideal Bayliss and Taylor 40-dB $\overline{n} = 6$ design pattern error slopes. The measured error slopes are within 10% of the ideal values.

V. CONCLUSION

The MSPA antenna pattern performance measured at the NRL Compact Range Facility is in good agreement with the design predictions. With a reduction of phase errors through range tuning, azimuth sidelobes below 30 dB should be feasible. Key array antenna characteristics are compiled in Table V.

By interleaving two closely spaced arrays with the proper excitations, it has been demonstrated that dual-plane monopulse with Taylor/Bayliss excitations can be obtained. All array phase shifters are used in forming the sum pattern, thereby maximizing the possible transmit power for a given phase-shifter capability.

ACKNOWLEDGMENT

The author would like to thank his coworkers, P. Bertalan and D. Binsley, for their assistance during the development and assembly of the array hardware and M. Viggiano for his development of the beam-steering controller. He would also like to thank M. Parent and J. Valenzi of the Naval Research Laboratory for his assistance during antenna testing.

REFERENCES

[1] J. T. Branigan and M. W. Wronski, U.S. Patent 4 958 166, Sept. 18, 1990.
[2] J. T. Nemit, U.S. Patent 4 164 742, Aug. 14, 1979.
[3] T. T. Taylor, "Design of line-source antennas for narrow beamwidth and low side lobes," *IRE Trans. Antennas Propagat.*, vol. AP-3, pp. 16–28, Jan. 1955.
[4] E. T. Bayliss, "Monopulse difference patterns with low sidelobes and large angle sensitivity," BTL Memo MM-66-4131, Dec. 2, 1966.
[5] R. C. Laverick and P. R. Smith, U.S. Patent 3 636 563, Jan. 18, 1972.
[6] R. R. Kinsey, U.S. Patent 5 612 702, Mar. 18, 1997.
[7] R. Kinsey, "Monopulse stick phased array," in *Antenna Applicat. Symp.*, Allerton Park, Monticello, IL, Sept. 1995, pp. 1–30.

Richard R. Kinsey (M'56–SM'85–LS'94) received the B.S.E. degree from the University of Michigan, Ann Arbor, in 1953, and the M.S.E. degree from Syracuse University, Syracuse, NY, in 1961.

From 1954 to 1985, he was an Antenna Engineer and Manager of the Advance Antenna Design Group, General Electric, Syracuse, NY. He has been a Vice President and Director of Antenna Engineering at Sensis Corporation, DeWitt, NY, since its founding in 1985. His primary technical interests are phased-array antennas and associated microwave components.